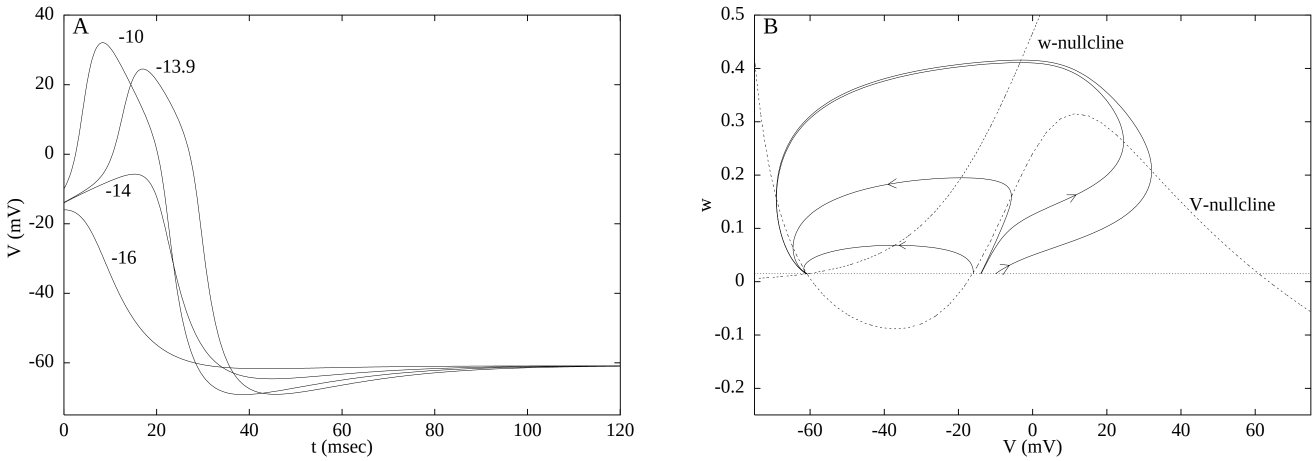

Figure 1: Response of the Morris-Lecar excitable system, equations (4-6), to a brief current pulse. For these parameters (see Appendix A), the system has a unique stable rest state, $\bar{V} = -61$ mV, $\bar{w} = .015$. The line $w = \bar{w}$ is shown lightly dashed. Four different stimuli lead to an instantaneous displacement of V from $\bar{V}$ to V_0 (values of V_0 are shown alongside the curves in **A**). **A** shows the time course of the voltage. Notice that intermediate responses are possible with some stimuli: the threshold is graded; firing occurs with finite latency. **B** shows trajectories in the $V - w$ phase plane; nullclines are shown dashed and intersect only once. The effect of a stimulus is to displace the initial condition horizontally from rest.

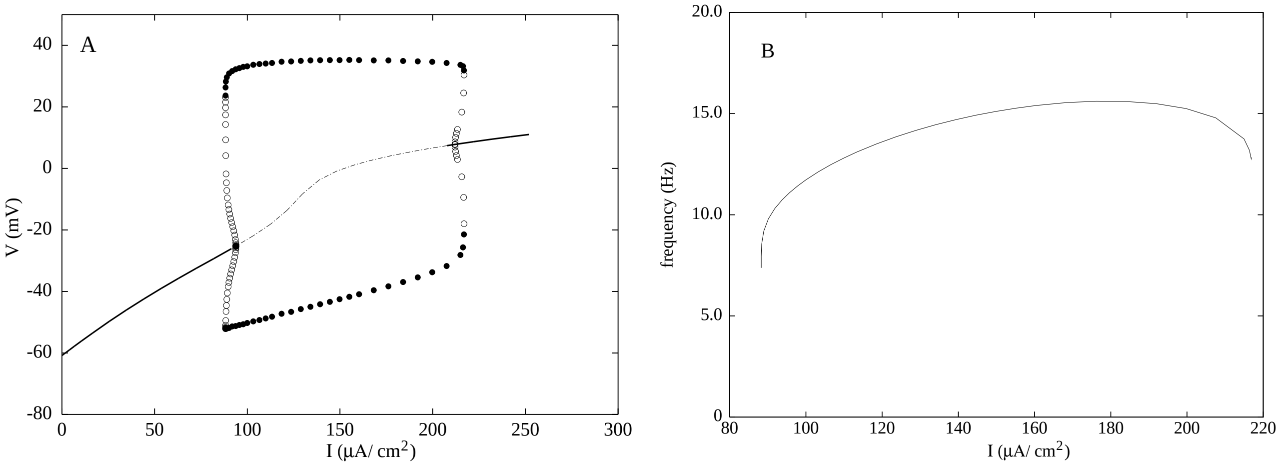

Figure 2: Repetitive firing in the Morris-Lecar model for steady current. Bifurcation diagram in **A** shows the steady-state voltage $\bar{V}$ versus I (thin lines; stable are solid, unstable are dashed) and the maximum and minimum voltage for periodic solutions shown as filled (stable) and unfilled (unstable) circles. The unstable branch of periodic solutions meets the branch of steady state oscillations at $I = I_1 = 94\ \mu A/cm^2$ and $I = I_2 = 212\ \mu A/cm^2$ (Hopf bifurcation points). The unstable branch of periodic solutions coalesces with the stable branch of periodic solutions at $I = I_\nu = 88\ \mu A/cm^2$. A similar coalescence occurs near $I = 215\ \mu A/cm^2$. For these parameters, the steady-state $I - V$ curve is monotonic. Furthermore, **B** shows that the frequency (plotted in Hz, and only for the stable limit cycles) as a function of current is always bounded away from zero. Parameters are as in Figure 1.

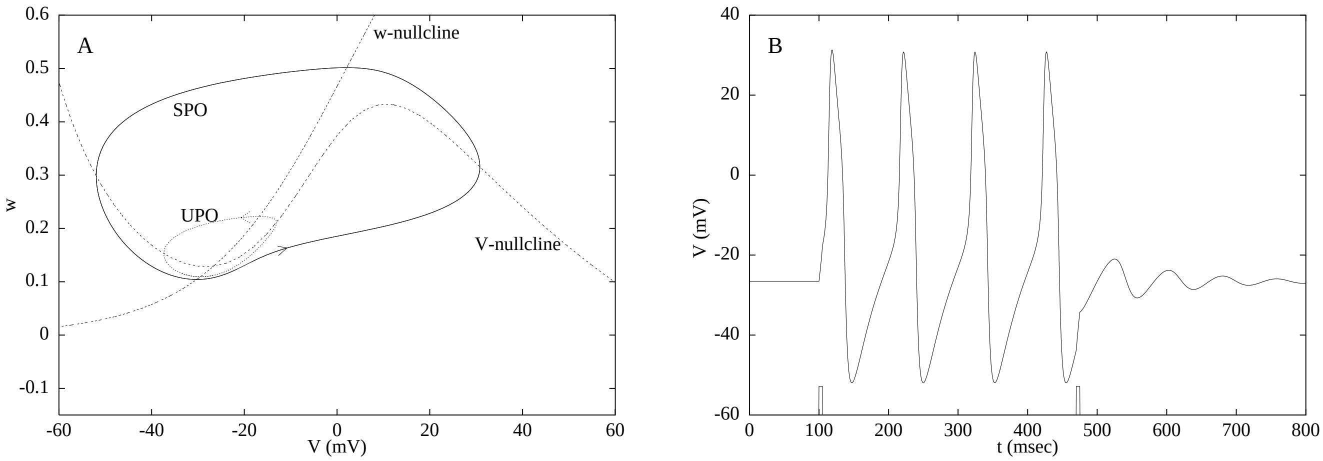

Figure 3: Bistability for steady current near the threshold for repetitive firing for the Morris-Lecar model with parameters as in Figure 1 and $I = 90\ \mu A/cm^2$. In this region, where I is between the first Hopf bifurcation point, I_1, and the "knee", I_ν, there are two stable states: a rest state (the intersection of the null-clines) and a stable oscillation (SPO) separated by an unstable periodic solution (UPO). This is shown in **A.** In **B** two brief appropriately timed depolarizing current pulses (shown in the figure) demonstrate switching from rest to oscillation and then back to rest.

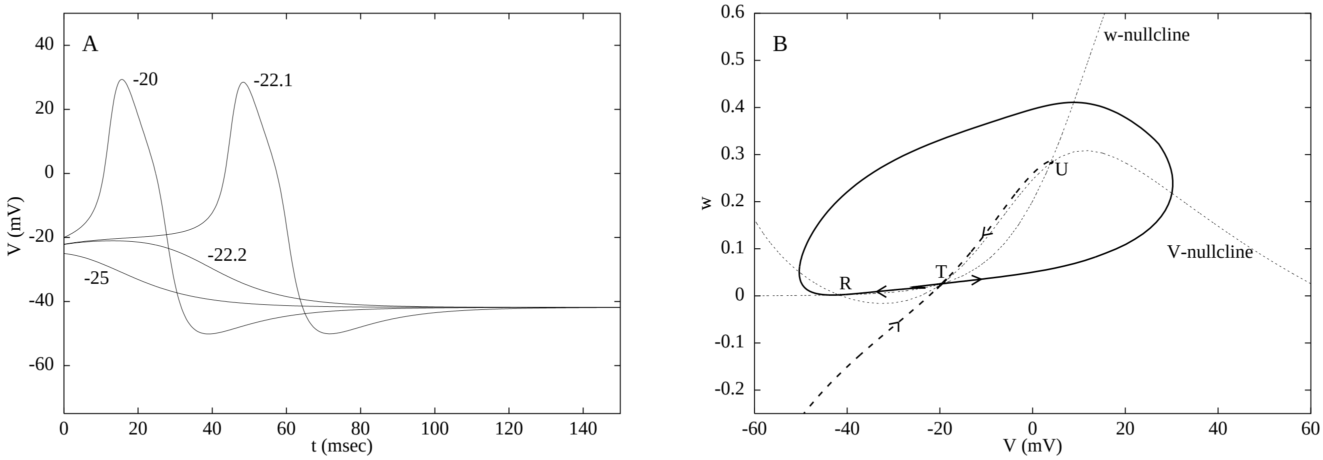

Figure 4: Excitability with three steady states and a distinct threshold; the response of the membrane to a brief current pulse from the stable rest state. Four different stimuli result in a displacement of V from $\bar{V}$ to V_0 (values of V_0 are given alongside the curves in **A**). **A:** Time course of the voltage for $I = 30\ \mu A/cm^2$. **B:** Phaseplane for the dynamics illustrated in **A.** Nullclines intersect at three places: (i) R a stable rest state, (ii) T, a saddle-point threshold, and (iii) U an unstable node. The thick solid line shows the unstable manifold for the saddle point; here, unstable refers to movement in opposing directions away from T (indicated by arrowheads). The manifold's two branches lead to the stable rest state and form a smooth loop in phase space. The heavy dashed line shows the stable manifold for the saddle point (arrowheads pointing toward T). Any initial conditions to the left of this manifold decay to rest. Initial conditions to the right lead to an action potential before returning to rest. Parameters are as in Figure 1, except, $\bar{g}_{Ca} = 4\ mS/cm^2, V_3 = 12\ mV, V_4 = 17.4\ mV, \phi = 1/15$.

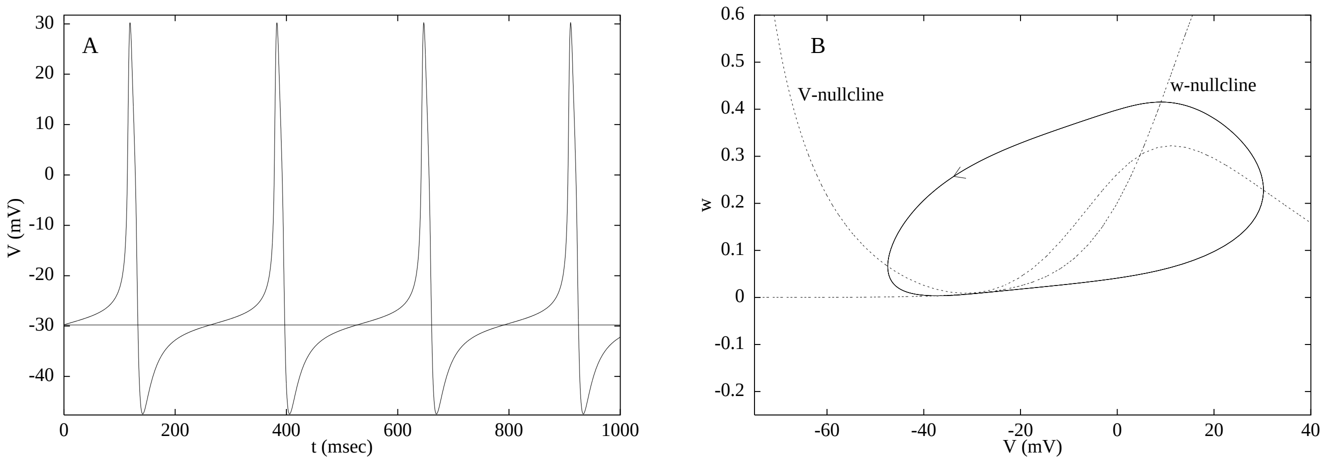

Figure 5: Onset of repetitive firing with arbitrarily low frequency for a constant current, $I = 40.76\ \mu A/cm^2$ shows an oscillation with a period of about 220 msec. **A** shows the voltage time course and **B** shows the phaseplane. Note the "narrow channel" between the two nullclines near -30 mV which accounts for most of the oscillation period (see [31]). Parameters are as in Figure 4.

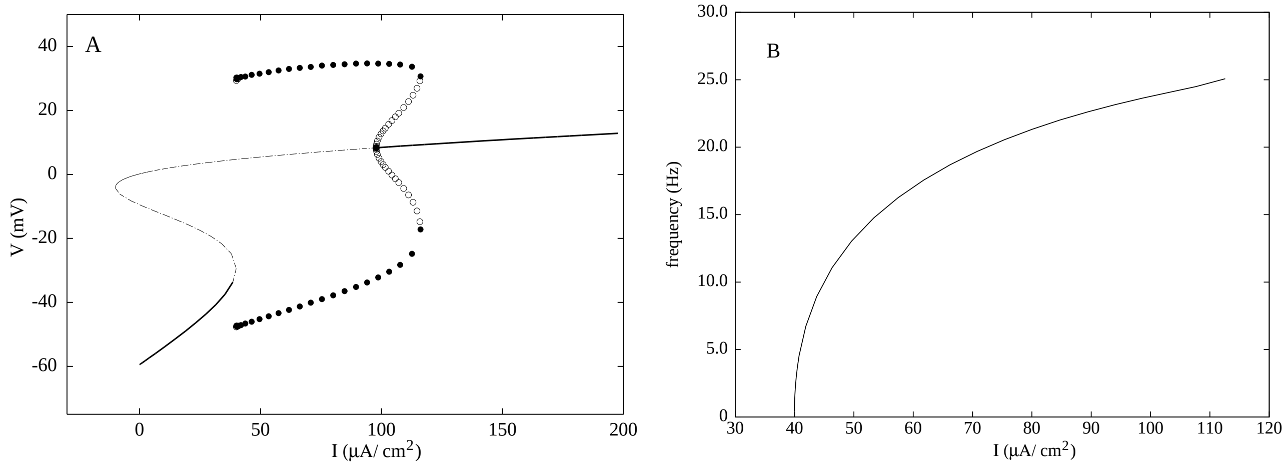

Figure 6: Multiple steady states and periodic orbits for a steady current when the I_{ss} vs. V relation is N-shaped. **A** shows the bifurcation diagram (line types as in Fig. 2A.) Parameters are as in Figs. 4, 5. In spite of the coexistent states, the system is monostable for I between $I_1 = 40$, the turning point of the steady states, and $I_2 = 98$ where there is a Hopf bifurcation. Onset of repetitive firing at zero frequency occurs at $I = I_1$ where two fixed points coalesce. This corresponds to Fig. 4B when the unstable manifolds of the saddle-point form a closed loop. The branch of periodic orbits has a turning point at $I = 116$ before terminating at the Hopf bifurcation point, $I = I_2$. All current values in $\mu A/cm^2$. **B** shows the frequency (in Hz) of the stable branch of periodic orbits.

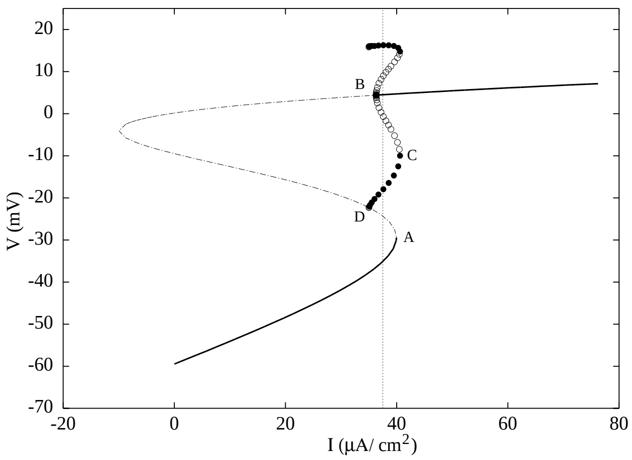

Figure 7: Bifurcation diagram as in Figure 6 but for $\phi = 0.23$. Point A shows where the two lower steady states coalesce, point B shows the Hopf bifurcation for the upper steady state, point C shows the coalescence of the stable and unstable periodic branches, and point D shows where the branch of stable oscillatory solutions terminates on the branch of saddle points (not on the knee as in Figure 6) at a saddle-loop homoclinic. For currents between points B and A, there are three stable states: (i) a low voltage rest state, (ii) a high voltage rest state, and (iii) an oscillatory state. Note that the steady state branch is identical to that of Figure 6; ϕ only affects the stability of the steady states and the behavior of the periodic orbits. Vertical line at $I = 37.5\ \mu A/cm^2$ shows a current for which there are 3 stable states (cf Figure 8.)

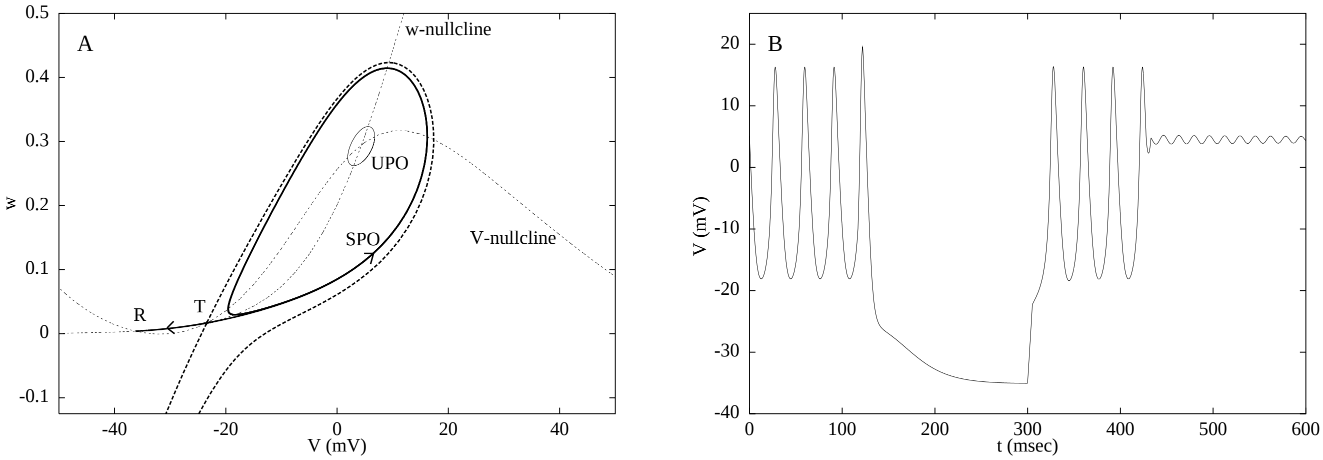

Figure 8: Multistability for a current between points B and A in Fig. 7. Here $I = 37.5\ \mu A/cm^2$; other parameters are as in Fig. 7. **A** depicts the $V - w$ phase plane. The nullclines intersect at three places representing steady states: (i) a lower stable rest state, (R), (ii) an unstable saddle point, (T), and (iii) an upper stable rest state (unlabeled). The left branch of the unstable manifold of the saddle point (bold line) connects to the lower steady state. The right branch wraps around the stable periodic orbit (SPO.) The branches of the stable manifold of the saddle point (bold dashed line) form a separatrix between the lower stable rest state and the stable periodic orbit. The unstable periodic orbit (UPO) separates the stable upper steady state from the stable periodic orbit. **B** shows the effects of three successive depolarizing current pulses. Starting on the stable oscillation, the membrane is switched to the lower stable steady state. Another brief pulse pushes it back to the stable oscillation and a third pulse switches it to the upper steady state. No single brief current pulse can switch it from the lower steady state directly to the upper steady state although the opposite transition is possible.

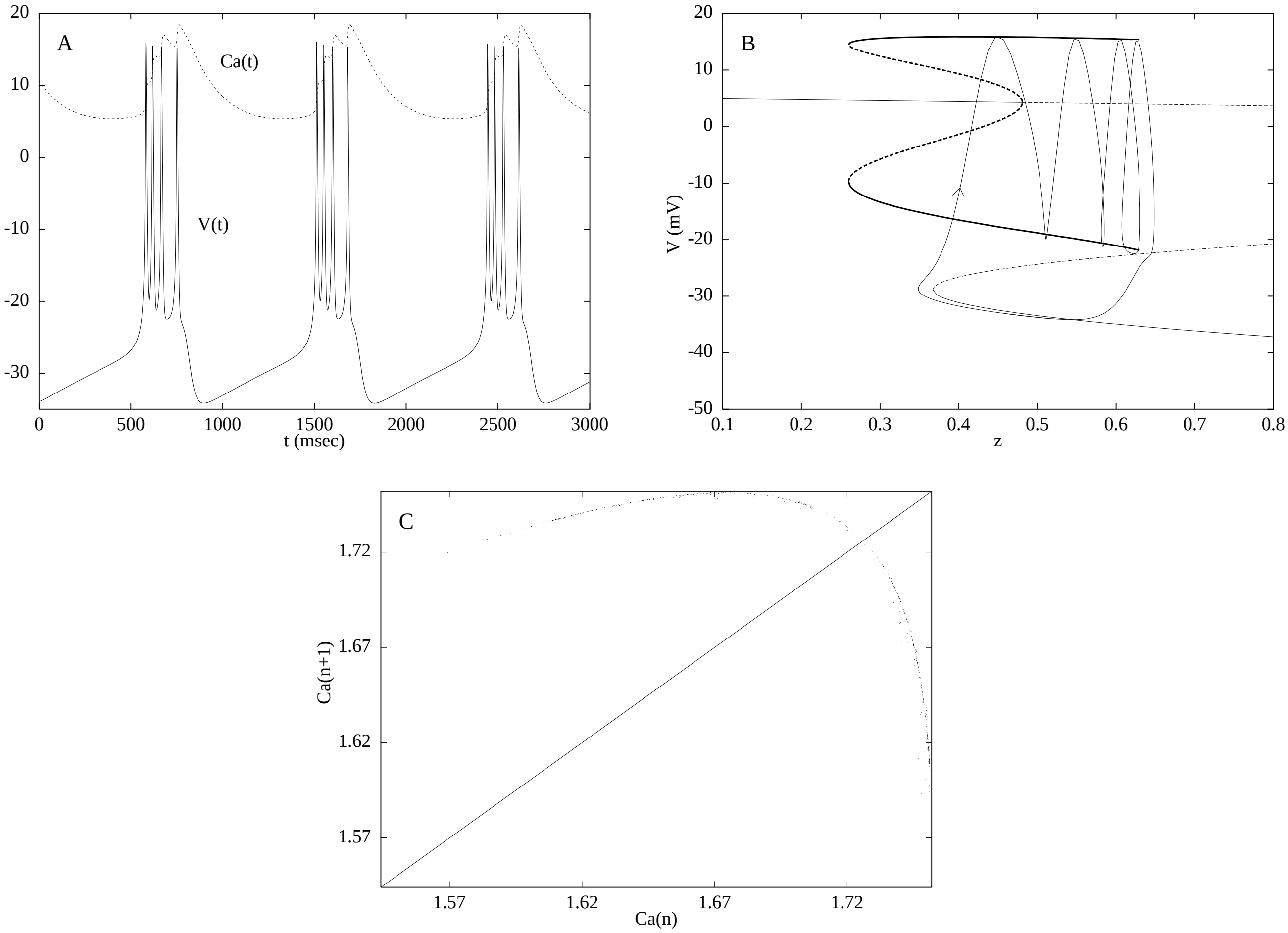

Figure 9: Bursting solution to equations (4-6) coupled with the calcium dependent potassium current, equations (20-22). Parameters are as in Figure 7, with $I = 45\ \mu A/cm^2, \epsilon = 0.005, \mu = 0.02, g_{K-Ca} = 0.25\ mS/cm^2$. **A** shows the voltage trace (use mV for ordinate scale) and the calcium concentration (for plotting clarity, the dimensionless Ca values have been multiplied by ten; unitless ordinate scale in this case). The burst's active phase ends when calcium rises too high and the membrane hyperpolarizes. During the silent phase calcium is removed and after the calcium-dependent potassium current diminishes enough the membrane depolarizes to initiate the next burst. **B** shows the projection of the bursting solution on the $z - V$ plane along with the bifurcation diagram with $z = Ca/(1 + Ca)$ as a parameter. The trajectory alternately tracks the stable periodic solution (SPO in Figure 8a) and the lower steady state. **C** For a slightly different value of $\mu = 0.01667$ the solution is chaotic. This figure shows the value of calcium at successive times as the voltage decreases through 0 mV. The solid diagonal line is the identity function. (See text for details.)

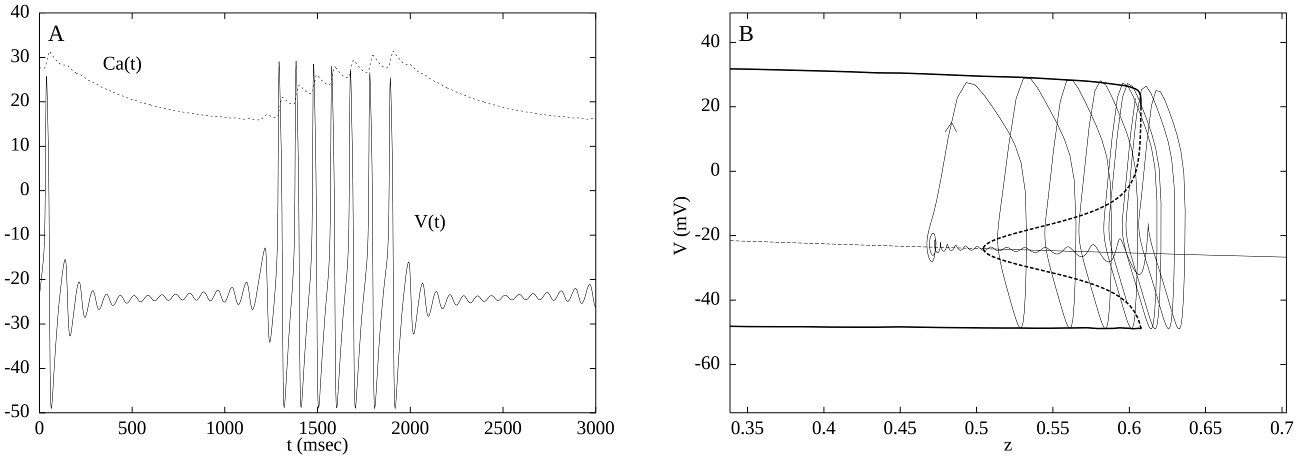

Figure 10: Elliptic burster formed when the Morris-Lecar model, equations (4-6) in the parameter regime of Figure 2, is coupled to the calcium-dependent potassium current, equations (20-22). Parameters are as in Figure 2 with $I = 120\ \mu A/cm^2, \mu = 1/60, \epsilon = 0.002, g_{K-Ca} = 0.75\ mS/cm^2$. **A** shows the time courses of voltage and calcium (ordinate scales as in Fig. 9A). As in Fig. 9, when the calcium is high and the calcium-dependent potassium channel is activated, the membrane tends toward rest and at low enough calcium it is oscillatory. **B** shows the projection of the burst on the $z - V$ plane as in Fig. 9B. During the active and silent phases, the burst trajectory slowly tracks attractors of the fast subsystem. Actually, the trajectory drifts, during the later phase of the silent period, well into the unstable regime of the fast subsystem's rest state (left of the Hopf point, $z < 0.5$), and this feature is explainable.

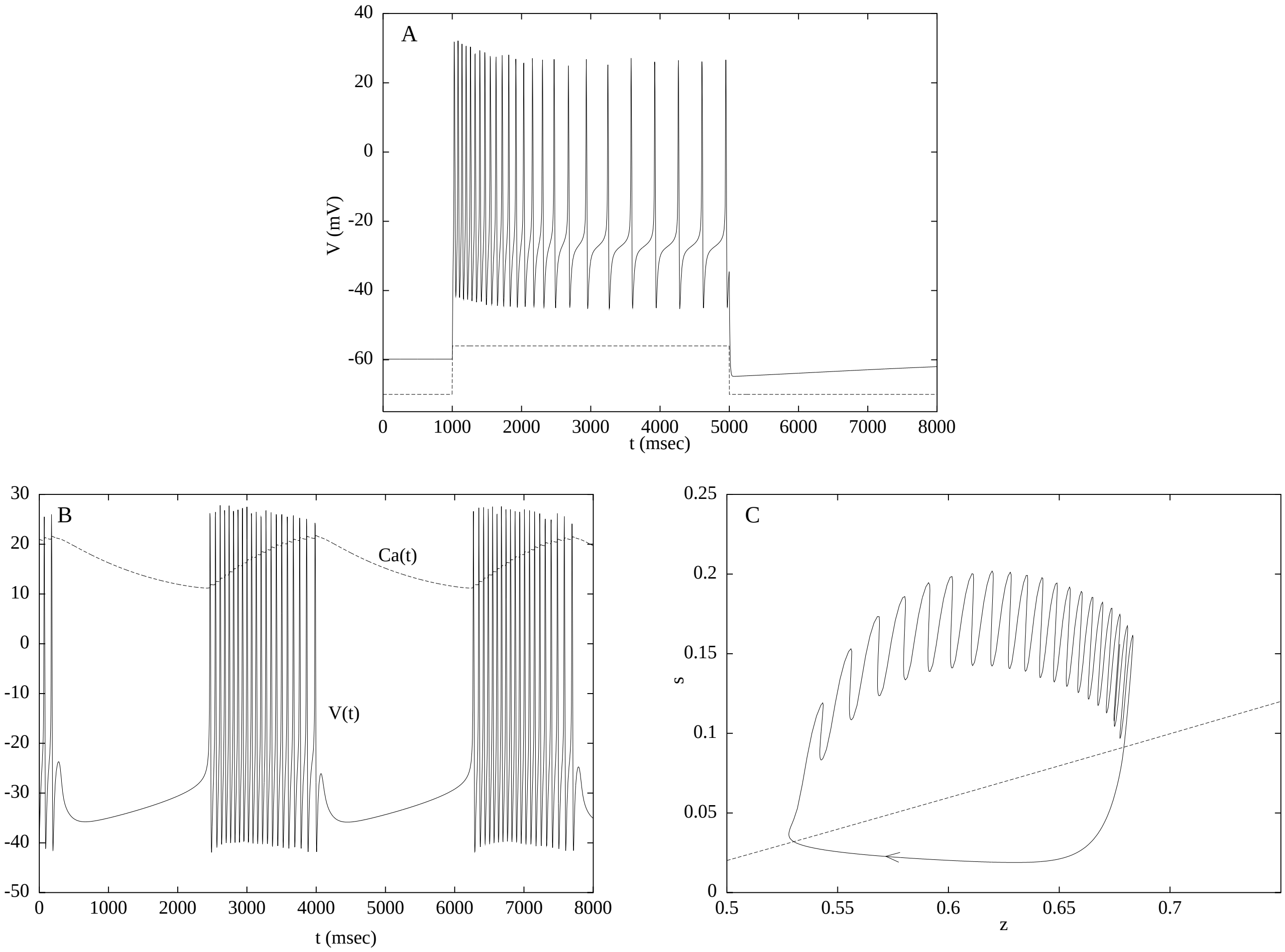

Figure 11: Modulation of the Morris-Lecar model, equations (4-6) in the regime of Figure 4, by slower processes. **A** shows how coupling with the calcium-dependent potassium current, equations (20-22), results in adaptation to a long current pulse. Parameters are as in Figure 4 with $g_{K-Ca} = 1\ mS/cm^2, \mu = 0.025, \epsilon = 0.0005$. The current pulse is 70 $\mu A/cm^2$. The membrane initially fires repetitively at 17 Hz and eventually slows to 3 Hz, more than a five-fold decrease. **B** A parabolic burster formed by adding an additional slow inward current governed by eq 23 with $I = 65\ \mu A/cm^2, g_{Ca,s} = 1\ mS/cm^2, \tau_s = 0.05\ ms$. Other parameters are as in **A**. This plot shows the membrane potential and the dimensionless calcium concentration as functions of time (ordinate scales as in Fig. 9A). For plotting convenience, Ca has been multiplied by ten. **C** shows the projection of the burst onto the $z - s$ plane. The dashed line is the curve of saddle-node-loop bifurcations of the fast dynamics viewing s and z as parameters. When above this line, the membrane is oscillatory and below it, there is only a stable rest state.

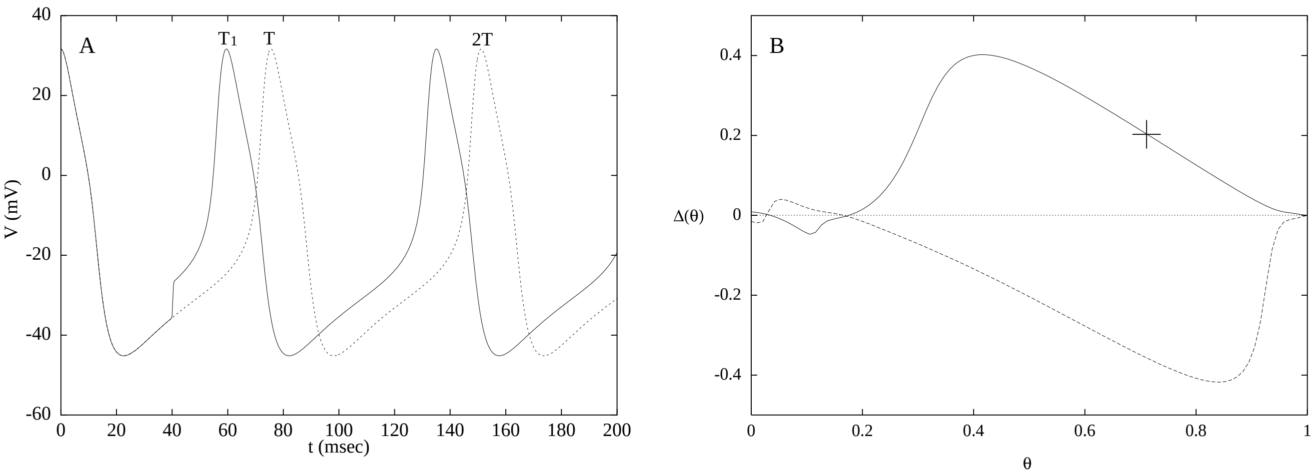

Figure 12: Phase resetting of a Morris-Lecar oscillator. **A:** A brief depolarizing stimulus can shorten the onset of the next spike and thus advance the phase. **B:** The phase response curve (PRC) for the Morris-Lecar equations with parameters as in Figs. 4-6 and an applied current $I = 45.6\ \mu A/cm^2$. The stimulus is a 0.5 msec pulse with amplitude of $\pm 480\ \mu A/cm^2$ delivered at time $t = 40$ msec. The solid line shows the PRC for a depolarizing stimulus and the dashed for a hyperpolarizing pulse. The cross on the depolarizing PRC corresponds to the experiment in Fig. 13.

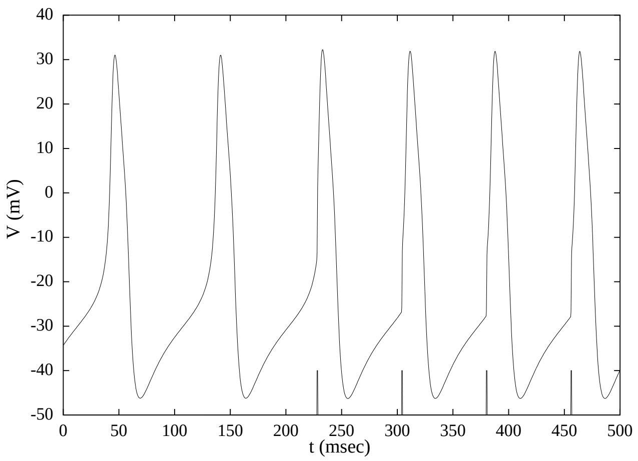

Figure 13: Phase locking (1:1) of the Morris-Lecar model to a series of four current pulses with interpulse period of 76 msec. Intrinsic period of the membrane oscillator is 95 msec. Parameters are as in Fig. 12b. After phase-locking is acheived, the stimulus is seen to occur about 67 msec after the action potential's peak, just as predicted by the PRC. (See text.)

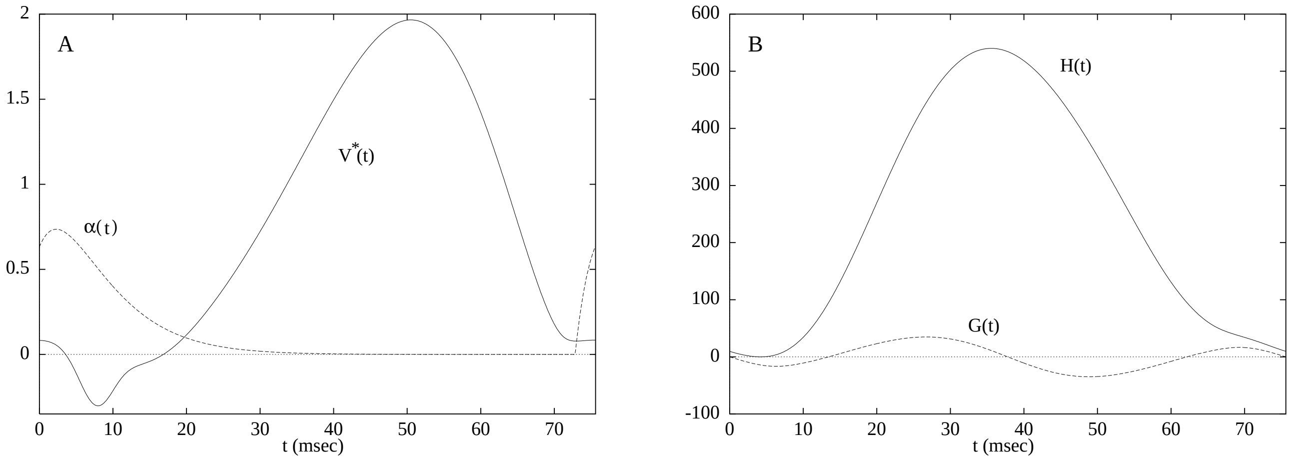

Figure 14: The method of averaging for two weakly coupled identical Morris-Lecar oscillators. Parameters for the oscillators are as in Figs. 4-6 (and Fig. 12A) and an applied current $I = 50\ \mu A/cm^2$. **A:** Solid line shows the infinitesimal PRC, $V^*(t)$ and the dashed line shows the time course of the excitatory synaptic conductance (for plotting convenience, here multiplied by ten), modeled as an alpha function with a 5 msec time constant and peak of about 0.075 mS/cm^2. The alpha function "turns on" when V crosses 20 mV. **B:** shows the interaction function $H(t)$ and its odd part $G(t)$ for the synaptic dynamics shown in **A** and a synaptic reversal potential of 0 mV. Zeros of the function $G(t)$ correspond to phase-locked solutions to the weakly coupled system; stable solutions have positive slopes and unstable have negative slopes.